# Emission features and expansion dynamics of nanosecond laser ablation plumes at different ambient pressures

N. Farid,[1,2] S. S. Harilal,[1,a)] H. Ding,[2] and A. Hassanein[1]

[1]*Center for Materials Under Extreme Environment, School of Nuclear Engineering, Purdue University, West Lafayette, Indiana 47907, USA*
[2]*Key Laboratory of Materials Modification by Laser, Ion and electron Beams, School of Physics and Optical Engineering, Dalian University of Technology, Dalian, China*

The influence of ambient pressure on the spectral emission features and expansion dynamics of a plasma plume generated on a metal target has been investigated. The plasma plumes were generated by irradiating Cu targets using 6 ns, 1064 nm pulses from a Q-switched Nd:YAG laser. The emission and expansion dynamics of the plasma plumes were studied by varying air ambient pressure levels ranging from vacuum to atmospheric pressure. The ambient pressure levels were found to affect both the line intensities and broadening along with the signal to background and signal to noise ratios and the optimum pressure conditions for analytical applications were evaluated. The characteristic plume parameters were estimated using emission spectroscopy means and noticed that the excitation temperature peaked $\sim$300 Torr, while the electron density showed a maximum $\sim$100 Torr. Fast-gated images showed a complex interaction between the plume and background air leading to changes in the plume geometry with pressure as well as time. Surface morphology of irradiated surface showed that the pressure of the ambient gas affects the laser-target coupling significantly. © *2014 AIP Publishing LLC.* [http://dx.doi.org/10.1063/1.4862167]

## I. INTRODUCTION

Laser-produced plasma (LPP) is a rich source of ions, electrons, neutrals, and excited particles and emits strongly in the visible, ultraviolet (UV), extreme UV, and x-ray regions of the electromagnetic spectrum. Some of the prominent applications of LPP include Pulsed laser deposition (PLD),[1] laser-ablation inductively coupled-plasma mass spectrometry (LA-ICP-MS),[2] laser-induced breakdown spectroscopy (LIBS),[3] nano-particles generation,[4] ion source,[5] and table top shorter wavelength light sources for lithography and microscopy.[6,7] Typically LPPs expand adiabatically and freely into vacuum; however, the presence of an ambient atmosphere modifies the entire process of plasma generation and hydrodynamic expansion. For example, the nature and pressure of an ambient gas greatly influence the energy coupling to the target, the laser-plasma coupling, and determine the hydrodynamic expansion features, cooling, and characteristic parameters (electron density, temperature) of the plume.[8] For most of LPP applications, a background gas with a certain pressure is typically added for a specific role in each application, e.g., an ambient gas is used to moderate the ions in PLD,[9] for controlling the debris in EUVL light source,[10] for rapid cooling of ablation plumes which leads to aerosol formation and flushes the aerosols to ICP torch in LA-ICP-MS,[11] and to confine the plume which enhances the optical emission in LIBS.[12]

The interaction of a nanosecond laser ablation plume with an ambient gas has been studied extensively in the past.[9,10,12–18] However, in spite of large number of reports available in the literature, studies of LPP interaction with ambient gas have not yielded conclusive results and this is due to various complex interaction taking place at different pressure levels between the expanding plume species and background gas species. Compared to vacuum, the interaction of LPP with a background gas becomes complicated because of involvement of new processes, such as reduction in ablation, formation of shock waves and clustering, plume splitting and sharpening, deceleration and confinement of ablated species, thermalization of the ablated species, diffusion, etc.[19–25] Background pressure levels also play an important role on the morphology of the laser irradiated region and evolution of LPP.[8] In nanosecond laser ablation, plasma shielding is one of the most important factors that control the ablation as well as the emission, and the nature and pressure of ambient gas have a definite role in controlling the shielding effect.[26,27] Hence, the observed plasma emission intensity dependence on background pressure is extremely complicated because of the changes in laser-target and laser-plasma coupling in the presence of an ambient.[28] It has been reported that at particular pressures, the plasma plumes emit profoundly in the presence of Ar compared to He or air.[29] The excitation temperature of the plasma plume has also a strong dependence on nature and pressure of the ambient gas.[12,30] In general, the emission intensity and plasma lifetime decreases with reduction in ambient pressure levels due to decrease in collisional excitation and ambient confinement, and the signal to background ratio is improved due to the reduced continuum radiation.[31] The presence of ambient gas also leads to generation of ambient plasma, and it has been noticed previously that the laser plasma from the irradiated target preceded by partially ionized ambient plasma.[32]

Characterization of laser ablation and behavior of resulting plasma formation under different background pressures

a)hari@purdue.edu

is significantly important for most of the applications. In this article, we report a comprehensive view on the background pressure effects on laser ablation, emission and expansion dynamics, temperature and density, morphology of the laser treated area, and analytical metrics. We used a multitude of diagnostic tools for this study, which include time resolved optical emission spectroscopy, plume imaging, ion analysis using Faraday cup, and crater surface morphology analysis.

## II. EXPERIMENTAL SETUP

The details of the experimental set up is given elsewhere.[32,33] Briefly, an Nd:YAG laser operating at 1064 nm, with a pulse duration of 6 ns at full width at half-maximum (FWHM), was used for laser ablation and plasma formation. High purity copper (99.995%) target was used for generating plasma. The target was mounted on an XY translational stage, which provided fresh surface for each laser shot. Whole experiments were performed in a high vacuum chamber with a base pressure $\sim 10^{-6}$ Torr. The laser beam was passed through a quartz window of the chamber and focused normal to the target surface using a plano-convex lens with a focal length of 40 cm. Laser energy was attenuated to 100 mJ on the target surface by using a combination of half wave plate and cube polarizer and the estimated spot radius at the target surface was 300 $\mu$m. This configuration gives a power density of $5.9 \times 10^9$ Wcm$^{-2}$ at the target plane.

For time resolved optical emission studies, a 0.75 m triple grating (3600, 1800, and 150 lines/mm) spectrograph was used. The spectrograph was coupled to an intensified CCD (ICCD) camera, which collected the wavelength dispersed spectral features of the plasma at the detector plane. For fast-gated imaging, the integrated visible emission from the expanding plasma was collected normal to the direction of expansion using a combination of a telephoto objective lens and an ICCD camera. The timing between the incident laser pulse and detector system was controlled by a programmable timing generator. The ion emission from the laser plasma were collected using a Faraday cup (FC) positioned at 16 cm from the target surface and at an angle 12° with respect to the target normal. A scanning electron microscope (SEM) was used to characterize the laser-generated craters at various pressure levels.

## III. RESULTS AND DISCUSSION

### A. Ambient gas effects on plume spectral features

Visible emission spectroscopic analysis has been carried out at various pressure levels for investigating the role of ambient gas on excitation of the plasma species. Typical time-resolved and time-integrated spectra recorded at various pressure levels of air are given in Fig. 1. In Fig. 1(a), the time resolved emission spectra from laser-produced Cu plasma in vacuum ($1 \times 10^{-5}$ Torr) and at atmospheric pressure (760 Torr) are shown. A 10% of the gate delay was used as the integration time (gate width) for collecting the spectrum. The spectral features show that a significant continuum emission especially at early times for plasmas generated both in vacuum and air ambient and its persistence decreases considerably with delay time. However, the intensity and persistence of the continuum emission are significantly enhanced in the presence of air ambient. Also at shorter time delays, ionic species are predominant, but for shorter time delays exceeding 150 ns, excited atomic emissions are evident along with ions in vacuum. Three characteristic lines of Cu I at 510.55 nm, 515.32 nm, and at 521.82 nm with strong emission intensities are clearly observed at later times. The distinct features of ns laser ablation spectra compared to ultrafast laser ablation plume spectra are the presence of ionic lines along with intense continuum at early times of plume generation ($<$100 ns).[34] In ns LPP, the leading edge of the laser pulse ablate the target and produce a vapor plume which contains electrons, ions, and excited neutrals, but the rest of the laser pulse is then utilized for heating and further ionizing of the plume leading to intense continuum generation at the earliest times. Along with continuum, the emission intensity from the all lines is increased significantly at atmospheric pressure compared with expansion into vacuum environment as shown in Fig. 1(a). Typical time integrated laser produced Cu spectra at different pressure levels are given in Fig. 1(b). An integration time of 1 $\mu$s with a delay of 100 ns was used to acquire the spectra, and all the measurements were done at a distance of 1 mm. Highest background was observed at 760 Torr, while this background intensity decreased with the reduction in ambient pressure levels. At higher pressures, the presence of ionic (444.7 nm,
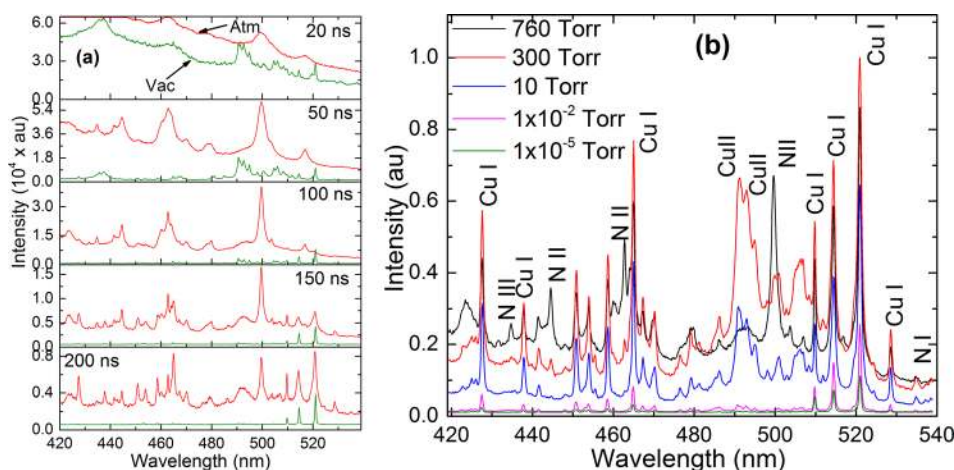


FIG. 1. (a) Time resolved emission features of laser-produced Cu plasmas in vacuum and at atmospheric pressure. A gate width of 10% of the delay time was used for the time resolved study. (b) Representative emission spectra of Cu plasmas at different background pressures are given. The spectra were acquired at a distance 1 mm from the target and with an integration time of 1 $\mu$s after 100 ns delay.

462.13 nm, 500.14 nm) and neutral (535.6 nm) lines of ambient gas (nitrogen) can also be clearly seen in the ns LPP.

Fig. 2 represents the peak intensity (line intensity plus background continuum) variation of a characteristic Cu I line at 510.5 nm ($4p^2P_{3/2}$-$4s^2D_{5/2}$) recorded at 1 mm from the target at various ambient air pressures. The plasma plume expands adiabatically in vacuum and undergoes free expansion. Hence line intensities are lower at vacuum conditions. However, line intensities grow with increasing pressure and attain a maximum value near to atmospheric pressure levels, and then decrease again with further increase in pressure. By increasing the pressure from $10^{-5}$ to 600 Torr, more than 20 times signal enhancement was noted in the peak intensity for the Cu I line at 510.5 nm. Although ∼100–600 Torr pressure levels are necessary to get the maximum signal intensity, it has to be mentioned that along with line intensities the background continuum also enhanced with increasing pressure (Fig. 1(b)). The reduction in line intensity at higher pressure can be explained by considering energy dissipation of plume by non-radiative ways, i.e., enhancement in collision of plasma species with the ambient gas resulting into increase of the extent of background continuum radiation. It is similar to that we have observed in ionization of ambient gas enhanced with increasing the background pressure, as shown in the Fig. 1(b).

Along with line signal intensity and continuum enhancement, the ambient pressure levels also affect the broadening of all spectral lines in the plume. The broadening, profile shapes, and line shifts of the spectral lines provide important information related to the emitter (atoms or ions) as well as the density of the plume. As showed in Fig. 2(b), the background pressure levels significantly influenced the shape and broadening of the emission line. Typical mechanisms that lead to broadening of a line are Doppler, Stark, and instrumental broadening.[35] The Doppler broadening produced due to the random thermal motion of the emitter and can be estimated by[36]

$$\Delta\lambda_{1/2} = 2\lambda\sqrt{\frac{2kTln2}{mc^2}}, \tag{1}$$

where $\lambda$ (nm) is the wavelength of transition line, $T$ (K) is the excitation temperature the transition, $m$ (kg) is the atomic mass, and c is the speed of light. For the Cu I line at 510.5 nm, the estimated width was ∼0.003 nm and hence the contribution from Doppler effect can be safely neglected.

The emitting species (atoms or ions) in the plasma are under the influence of an electric field by fast moving electrons and relatively slow moving ions. This perturbing electric field can act on atom or ions by shifting their energy levels which can broaden the emission lines, known as Stark broadening.[35] The Stark broadened line width without ionic contribution is given by[37]

$$\Delta\lambda_{1/2} = 2W\left(\frac{N_e}{10^{16}}\right), \tag{2}$$

where $N_e$ (cm$^{-3}$) is the electron density and W (nm) is the electron impact width parameter. The line profiles contributed by Doppler and Stark effects are typically given by Gaussian and Lorentzian profiles, respectively. The spectrographs also contribute the broadening of a spectral line called instrumental broadening. Since instrumental broadening also exhibits Lorentz shape, the instrumental broadening can simply be subtracted by deconvolution process[37]

$$\Delta\lambda_{stark} = \Delta\lambda_{tot} - \Delta\lambda_{inst}. \tag{3}$$

Typically the Stark effect is the main contributor for line broadening in the laser plasmas which is given by a Lorentzian profiles. For recording the spectral broadening caused by the ambient gas effects, we operated the spectrograph at its highest resolution (∼0.015 nm) by keeping minimal slit width and by selecting 3600 l/mm grating. The Lorentzian fitted profiles are also given in Fig. 2(b) along with recorded spectra. In general, an increase in broadening was observed with increasing ambient pressure caused by the Stark effect. This suggests that the density of the plume is related to the ambient pressure levels, which may be influenced by confinement effects, the laser-target coupling, and plasma shielding.

### B. SNR and SBR estimate

Addition of ambient gas provides collisional excitation to all plume species, and hence it leads to enhancement in signal intensity from all emission lines. However, along with line intensity, both the background (continuum) as well other noise levels are also increasing. So it is very important to know signal to noise (S/N) and signal to background (S/B) ratios especially using laser ablation plumes for analytical applications. S/B and S/N ratios have been calculated using the peak intensity, $I_p$, of the 510.5 nm Cu I line, the averaged
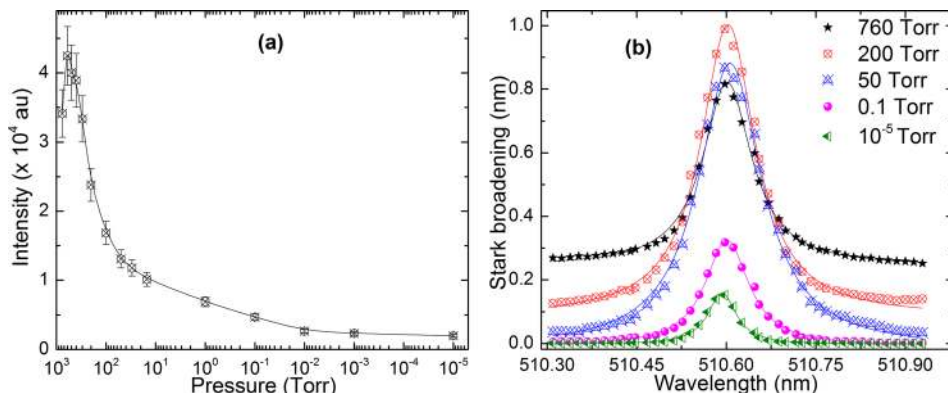


FIG. 2. (a) Variation in peak intensity of spectral line Cu I at 510.5 nm and (b) in Stark broadening with pressure. The experimental data points are represented by symbols while solid lines represent Lorentzian fitting. All the spectra were acquired with integration time of 1 μs after 100 ns delays.

background intensity, $I_b$, on the higher and lower wavelength sides of the line, and the times the standard deviation ($3\sigma$) in a 1 nm region of spectrum where there is no emission line according to the following equations:[38]

$$\frac{S}{B} = \frac{I_p - I_b}{I_b}, \qquad (4)$$

$$\frac{S}{N} = \frac{I_p - I_b}{3\sigma}. \qquad (5)$$

The estimated S/N and S/B ratios are given in Figure 3 for various delay times. As expected, both S/N and S/B ratios are changing with pressure. Even though the maximum peak intensity is observed at ~600 Torr (Fig. 2(a)), the optimum S/N and S/B ratios are noticed at lower pressure levels. Similar to line intensity changes with pressure, both S/N and S/B increases steadily with increase in pressure from $10^{-5}$ Torr and attain its maximum value ~10–30 Torr and then decreases with further increase in pressure. The observed S/N and S/B ratios are also strongly depended on gate delay with respect to the onset of plasma formation, and optimum values are obtained at 100 ns delay. The best S/B was found for a delay time of 100 ns at pressure of 30 Torr. However, the optimum S/B ratio for 150 and 200 ns delays were observed at 15 Torr. In comparison, at atmospheric pressure, about 1.9 × enhancement in S/B was obtained with 200 ns delay as compared to 100 ns delay and about 1.2 × to that of 150 ns delay. In contrast, the best S/B was observed at 100 ns delay in vacuum. This is due to low background emission (continuum) even at early times. The line intensities as well as continuum background intensities enhanced with an increase of background pressure. For example, for the case of 100 ns delay, the line emission was relatively higher ~100 Torr than ~30 Torr, but the large background continuum at ~100 Torr in effect decreased S/B value than at ~30 Torr pressure levels. Yalcin *et al.*[39] have studied the influence ambient air pressure on the optical emission from LPP using 130 fs laser pulses at 800 nm. At all investigated gate delays, they found the optimum values of S/B and S/N ratios at 4 Torr. The enhancement in S/N and S/B at low pressure was attributed to plasma cooling by background gas.

The optimum S/N and S/B ratios were obtained at a pressure of 30 Torr. A lower S/B ratio at atmospheric pressure levels (760 Torr) is due to the higher value of continuum

caused by plasma confinement. So even though the highest peak intensity is seen from the plasma at higher pressures (Fig. 2(a)), the presence of greater continuum suppressed the S/B values at higher pressures. The enhanced emission as well as continuum emission will have direct correlation with characteristic plume parameters (temperature and density). Hence, we estimated the excitation temperature ($T_e$) and electron density ($N_e$) of the plume using spectroscopic means at various pressure levels.

## C. Influence of pressure on $T_e$ and $N_e$

The variations of temperature and electron density with pressure are given in Fig. 4. Both the characteristic parameters of the plasma were measured at a distance 1 mm from the target with an integration time of 1 $\mu$s. Electron density was determined using the Stark broadening of Cu I line at 510.5 nm while the temperature was measured by Boltzmann's plot method using Cu I lines at 427.5, 465.1, 510.5, 515.32, and 521.82 nm. According to Fig. 4, as the pressure decreases from atmosphere, the temperature increases and then attain a maximum value at ~400 Torr and then decreases with further decrease in pressure. The variation of density with pressure is peaked at ~100 Torr and dropped either sides of this pressure level.

The increase in temperature of the plume from vacuum level to 400 Torr can be related to plasma heating by ambient confinement and enhanced laser-plasma coupling. When a nanosecond laser with high pulse energy interacts with a target, the entire laser pulse energy is not directly coupled with the target surface because of shielding effect. The effective coupling of the laser-target and laser-plasma depends strongly on the properties of incident laser (pulse duration, wavelength)[34,40] and also has a strong dependence on the ambient conditions (nature and pressure). The initially ejected material has low degree of ionization and continues to absorb energy (by the inverse Bremsstrahlung (IB) or multiphoton ionization) from the remaining laser pulse, resulting into shielding of the sample surface from the laser pulse.[41] In the IB, the free electrons absorb the photon from the incoming laser, which in turn increases the electron temperature and promotes ionization and excitation through collisions with the excited and the ground state neutrals. The IB coefficient $\alpha_{IB}$ (cm$^{-1}$) via free electron depends on the laser wavelength and given as[42]
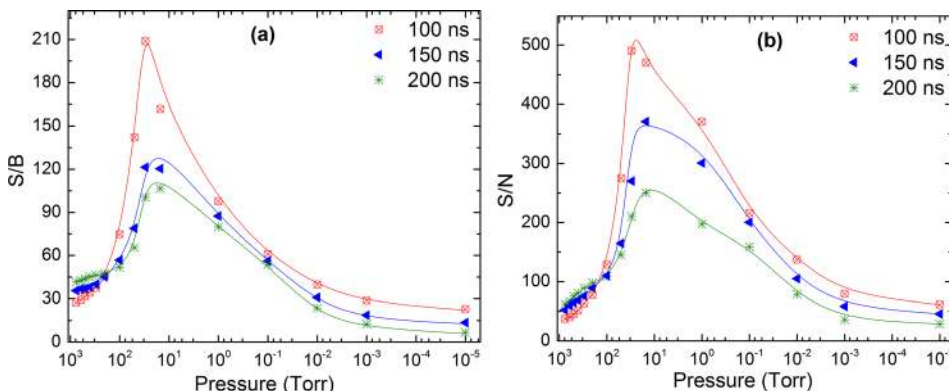


FIG. 3. (a) The S/B and (b) S/N as a function of background air pressure for Cu I emission line at 510.5 nm. Cu plasma was produced by ns laser pulses with $5.9 \times 10^9$ W/cm$^2$ intensity, and spectra were acquired using 1 $\mu$s gate width and 100 ns delays time.
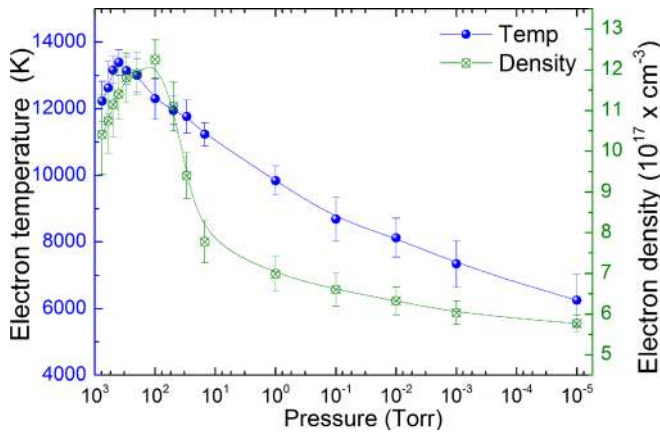
FIG. 4. The influence of background air pressure on electron density and temperature of Cu plasma. Temperature was measured by Boltzmann's plot using 427, 465, 510, 515, and 521 nm lines. The Stark broadened profile of Cu I at 510.5 nm was used to determine the density. Cu plasma was produced with a 100 mJ pulse energy and emission was acquired using a 1 $\mu$s gate width and 100 ns delay.

$$\propto_{IB} = 1.37 \times 10^{-35} \ \lambda^3 N_e^2 T_e^{-\frac{1}{2}}, \qquad (6)$$

where $\lambda (\mu m)$ is the wavelength of incident laser, $N_e$ (cm$^{-3}$) and $T_e$ (K) are the electron density and electron temperature, respectively. It is clear that IB is dominated at longer wavelength, as in our case (1064 nm). The second mechanism is photoionization (PI) of excited species by direct absorption of photons which become prominent with the shorter wavelengths lasers. The IB process also has a strong dependence on plasma density ($N_e^2$) and weak dependence on temperature. The addition of ambient gas leads to plume confinement and increase in density (Fig. 4), which in turn enhance the laser-plasma coupling through IB.

The shielding and confinement of plasma by background gas was dominated at higher pressure, resulting in an increase in energy gain in plasma from the incident laser pulse and hence generating hotter plasma. The energy that is coupled into the plasma through IB is directly proportional to the electron density, and hence at higher pressure, the amount of ablated mass could be less due to strong shielding. On the other hand, at higher pressures, the hot plasma loses its energy by collision and form shock waves into the background atmosphere. In short times, the rate of loss of electron energy to the background is mainly dominated by the elastic collision, given as[43]

$$Q_{\Delta t} = \frac{2m_e}{M_B} \sigma_{ea} n_B \left[ \frac{5kT_e}{\pi m_e} \right]^{\frac{1}{2}}, \qquad (7)$$

where $n_B$ and $M_B$ are the density and mass of the background gas, respectively, and $\sigma_{ea}$ represents elastic scattering cross section of the electrons. It means that the cooling is directly proportional to the density of background gas. Therefore, at higher pressures heating caused by the confinement and enhanced laser-plasma coupling can be compensated by the energy loss due to enhanced collisions.

## D. Ambient gas effects on laser ablation craters

Since the ambient conditions affect both laser-target and laser-plasma coupling, it can influence the properties of laser-produced craters. Fig. 5 shows laser treated Cu surface with 20 laser shots in vacuum and at an atmospheric air pressure under similar conditions that was used for the optical spectroscopy. The energy density used in this study (32 J/cm$^2$) was significantly higher than the melting damage threshold (3.3 J/cm$^2$)[44] and hence the ablation and crater formation was observed even after the first pulse. However, to improve the accuracy to make a clear distinction in craters produced in vacuum and under ambient pressure, 20 laser pulses were accumulated. Both in vacuum and at atmospheric pressure, the laser treated area can be divided into central intense melting region and a region around it where the melting material re-solidified in the form of microstructures. The common features at atmosphere and in vacuum are the re-solidification of molten material in the form of whirlpools or concentric vertical ridge, turbulence, droplets, nanopores, and re-deposition of particles. As the laser intensity is maximum at center and decreased towards periphery because of Gaussian distribution in the laser beam, it generates a temperature gradient which causes liquid material movement mainly along the radial direction resulting into formation of regular ridge (ripples) which spread up to the periphery of laser spot. Significant difference in the crater depth along with substantial splashing of molten material is prominent on the crater produced at atmospheric pressure than in vacuum. As mentioned earlier, at higher pressures, the plasma shielding becomes dominant which not only reduces the mass ablation but also absorbs the energy from the incoming laser resulting into higher temperature plasma in front of the target surface. This hot plasma may enhance
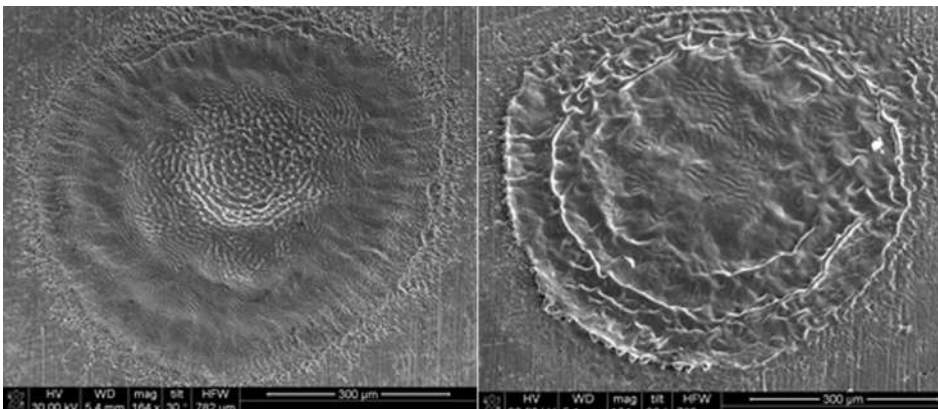


FIG. 5. SEM Micrographs revealing the Cu surface characteristics after irradiating by a 20 laser pulses with an energy of 100 mJ at 1064 nm wavelength in vacuum (left) and atmospheric pressure (right).

the pressure on the molten surface, which may cause the splashing and enhances the material movement from center to periphery of treated area, and this effect can be clearly seen in Fig. 5 (right). At higher pressures, plasma confinement is also taking place. This will increase the temperature of the plasma and hence the radiation heating of the target by the plasma which may affect the crater dimension and properties. It means the temperature of plasma produced in front of irradiated surface leaves the vital effect on the surface morphology.

SEM images also showed the more material removal at low pressure as compared to atmospheric pressure. However, the spectroscopic results provided smaller values of electron density at lower pressures compared to plasma generated in 1 atmosphere. In vacuum, the initially ejected material expands freely and the density drops rapidly.[45] It allows the incoming laser pulse to reach the target surface and enhance the material ablation resulting into higher crater depth in vacuum. Present results are also in consistence with the reported studies on ambient pressure dependence ablation rate where it was found that ablation efficiency strongly depended on the nature and pressure of background gas and enhances at lower pressure.[27]

### E. Ambient gas effects on plume hydrodynamics

Optical emission spectroscopy data suggest that peak intensity increases with pressure and maximum was observed at 600 Torr (Fig. 2(a)), while the best S/B was observed at 30 Torr. The estimated electron density and temperature peaked at 100 Torr and 400 Torr, respectively. In general, plasma temperature and electron density influence the line and continuum emission and surface structures of laser generated craters. The pressure of ambient gas does influence the hydrodynamics of plume expansion greatly, and hence we performed fast imaging of laser-ablated plumes under various ambient pressure conditions. Fast imaging of LPP plume is one of the simplest diagnostic techniques that provide the comprehensive details of hydrodynamic expansion as well as internal structures. Hydrodynamics expansion of LPP at different pressures ranging from vacuum to atmosphere was investigated by gated imaging employing ICCD camera. Images of the temporal evolution of plasma are taken at different air pressures ranging from $10^{-5}$ to 760 Torr. Typical ICCD images of the expanding plume at different times after the onset of the laser are given in Fig. 6 at different air pressures. All the images are spectrally integrated in the 350–900 nm region that contain the emission from the various species (i.e., excited neutrals and ions) and are normalized to maximum intensity of each image for a clear view. In vacuum, plume expands freely with cylindrical shape and followed an adiabatic expansion that has been predicted by the numerical simulation.[46] The interaction between the plasma and background gas is found to be minimal until $10^{-2}$ Torr considering the mean free path of the ambient gas species is significantly higher which limits the probability of collisions with expanding plume species. However, the plume gets brighter with increasing pressure >10 mTorr because of enhancement in collisions
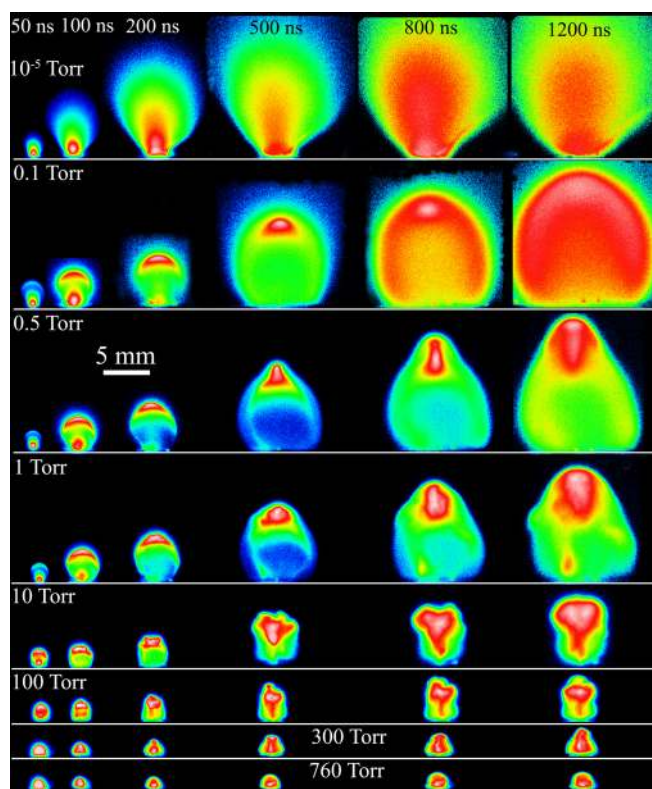


FIG. 6. Spectrally integrated and time resolved images of ns laser ablation of Cu obtained using an ICCD camera. All the images are captured using a gate width that corresponds to 10% of delay time and normalized to its maximum intensity.

with the background gas. When the pressure is increased to 100 mTorr, the plume breaks away from the target surface $\sim$50 ns after the laser onset, forming a faster moving component and a slow component near the target surface. Such a clear boundary separating plume and ambient medium has been noticed previously by several authors.[47,48] At this pressure, the plume expansion is more spherical in nature.

The plasma plume is found to be getting brighter with increasing pressure because of enhanced collisions with ambient species. At a pressure of $\sim$500 mTorr and for up to 200 ns delay times, the plume propagation seems to be quite similar to that at 100 mTorr. However, the plume front, which is spherical in nature at early times ($\sim$<200 ns), becomes sharpened as time evolves. Plume sharpening behavior are based on the fact that higher kinetic energy particles and ions with higher charge states dominate in the direction normal to the target, their concentration falls sharply away from the normal, and excited neutrals have the most angular spread.[49] At 1 Torr and up to 200 ns, the plume geometry was similar to that of 100 and 500 mTorr. However, at later times, the plume front shows some instabilities between the two mediums, and this phenomena is more evident at 10 Torr pressure levels. The confinement of the plume is found to be much rapid when the pressure increases from 1 Torr, and this leads to enhancement in collisions within the plume resulting increased density and recombination which in turn increase the persistence of all species in the plume.

At 10 Torr pressure levels, the pressure exerted by the background gas particles is higher and the ambient gas drag

the plume both in the radial and in the axial directions. Also at these pressure levels, along with deceleration the turbulence also appears in the expanding plume. The instabilities at the interface of two fluids (i.e., plasma and ambient gas) are probably caused by the Rayleigh-Taylor instability. Similar turbulence has been observed by previously by several authors.[25,50] Interestingly, the highest S/N and S/B ratios were noticed at these pressure levels. However, it has to be mentioned that all the spectral measurements were made at a distance 1 mm from the target surface where intensity striations are minimal according to ICCD images. At higher-pressure levels ($\geq 100$ Torr), the plume is compressed by the background gas both in the radial as well as in the forward direction, the energetic species in the plume tend to succeed the confined region through a diffusion-like propagation which can be seen clearly at 100 ns at 100 Torr pressure. At this pressure levels, the turbulence are enhanced and the instability are start to manifest even at early times. At still higher pressures ($\sim > 100$ Torr), a greater confinement of the plasma takes place and the effective length of the plume is reduced to a few millimeters. The recorded plume temperatures and densities were found to be maximum at these pressure levels (100–300 Torr).

Several previous studies have been reported on the expansion and dynamics of LPP plume in background gas and observed that the dynamics of plume is greatly affected by the background pressure. Amruso *et al.*[51] investigated excimer laser ablation of a LaMnO$_3$ and studied the effect of reactive background gas (oxygen) pressure on the expansion dynamics of the plasma and its interaction with background to form oxides. The expansion dynamics of the plume front is explored by theoretical model and shock-wave propagation in dimensionless variables. Similarly, Lafane *et al.*[47] studied the expansion dynamics of Sm$_2$O$_3$, Nd$_2$O$_3$, and NiO in oxygen atmosphere using KrF laser at a pressure ranging from vacuum to 50 millibars and observed the double plume splitting, plume sharpening, and plume stopping. A comparison of reactive and non-reactive gases suggests that shock-velocity, strength, and its structure are strongly dependent on nature of ambient gas and its pressure. Shock with higher velocity was produced in helium than argon.[52] We used plume images to create the position-time (R-t) plots in order to explore more about the expansion dynamics of LPP at different pressures, and results are given in Fig. 7. The symbols represent the experimental data points and the curves represent fitting to different expansion models. In vacuum, the plume expands freely and follows the R $\alpha$ t as given by a straight-line fit in Fig. 7. The plume expansion at 0.5 Torr is represented by a shock model, which is given by R = £$_o$ (E$_o$/$\rho_o$)$^{1/5}$ t$^{0.4}$, where £$_o$ is a constant and dependent on the value of specific heat, E$_o$ is the amount of energy released during the shock to the background having $\rho_o$ density. At higher pressures, the plume expansion is better described by a drag model, which is given by R = R$_O$ (1-exp (-$\beta t$)), where R$_0$ is the stopping distance of the plume and $\beta$ is the deceleration coefficient (R$_o\beta = v_o$). The deceleration coefficient changed from 0.0031 to 0.0041 ns$^{-1}$, as the pressure increases from 1 to 300 Torr.

Plume images are representative of emitting species, and it is not necessary that all species in the plasma are
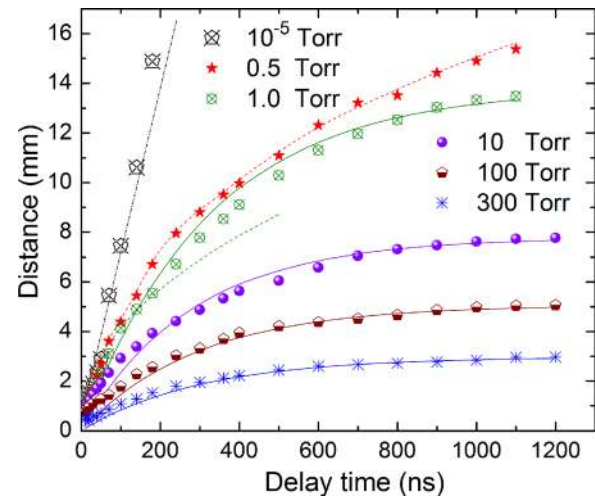


FIG. 7. Plume front-time (*R- t*) plots for the laser-produced Cu plasma plume at different background air pressures measured from ICCD images. Experimental data points are represented by the symbols while the curves represent different expansion models. The straight solid line represents the free expansion in vacuum, which follow the R $\alpha$ t. The dashed curves represent the shock wave model (i.e., R $\alpha$ t$^{0.4}$) for 0.5 and 1 Torr. The solid curves show the drag model fit with $\beta = 0.0031$ for 1 Torr, 0.0036 ns$^{-1}$ for 10 Torr, 0.0039 ns$^{-1}$ for 100 Torr, and 0.0041 ns$^{-1}$ for 300 Torr.

emitting in the visible region. So we recorded ion kinetic energy profiles using a Faraday cup and compared with results obtained from ICCD imaging at vacuum conditions. The FC was placed at angle of 10° to target normal and 16 cm from the target surface. A bias voltage of −30 V was applied to the FC to repel the electrons and accelerate the ions. Typical ion signal along with KE profile obtained from the FC ion signal is given in Fig. 8. The estimated maximum probable KE from the FC signal is $\sim$1.76 KeV. The maximum velocity of ions measured from FC was $7.3 \pm 0.7 \times 10^6$ cm s$^{-1}$, which was higher than the velocity $(4.2 \pm 0.18 \times 10^6$ cm s$^{-1})$ of plume in vacuum estimated by the ICCD images. It implies that the fast moving ions in the plasma plume are not emitting in the visible region of the electromagnetic spectrum.

Modeling or simulation approaches has also been carried out in order to investigate the interaction LPP with the background gas; a model based on the spherical expansion of plume has been used to study the hydrodynamics expansion of plasma from low to higher pressure.[53] This model based on the laws of mass, momentum, and energy conservation, formation and movement of internal and external shock wave, and prediction describe very well the experimental results. It was observed that at the first stage, plume expands freely as in vacuum, generation of internal and external shock waves causing the heating and deceleration of plume at intermediate stage, and finally, the stopping of plume. Recently, another model based on the gas-dynamical approach of Predtechensky and Mayorov (PM) provides a relatively simple description of complicated hydrodynamics of LPP plume.[54] They concluded that after stopping the plume in background gas, the initial kinetic energy of the plume is dissipated to background gas. This suggests that LPP releases a part of its energy, which could dissociate,
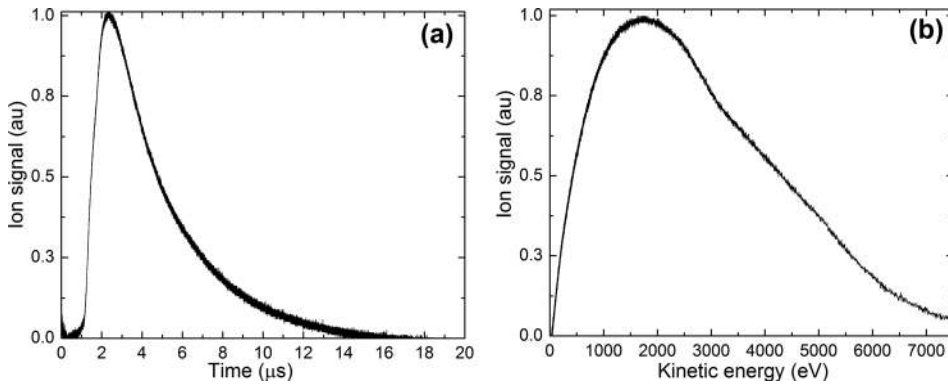
FIG. 8. (a) Typical ion TOF signal for Cu obtained from FC. FC was positioned at 16 cm from the target surface and at an angle of $10°$ to the target normal. (b) The KE profile of ions which gives 1.76 KeV as maximum probable KE of ions.

excite, and ionize the background gas resulting into enhancement of continuum background.

We also compared the experimentally measured plume length in different air pressures using the adiabatic expansion model. According to the adiabatic expansion model, plume expansion is stopped after a certain delay times when the plasma and background gas pressure equilibrate. Then, the stopping distance or length of plume is given by[55]

$$L = A \ [(\gamma - 1)E]^{1/3\gamma} P^{-1/3\gamma} \ V_i^{(\gamma-1)/3\gamma}, \quad (8)$$

where E is the laser energy, $\gamma$ is ratio of specific heats, P is the background pressure, and $V_i$ is the initial volume of the plume at the end of the laser pulse given by $V_i = \nu_o \tau a$, where $\nu_o$, $\tau$, and a are the initial velocity of plume, laser pulse width, and area of laser spot at the surface of target, respectively, and A is a geometrical factor, which depends on the expansion angle $\theta$. For a plume with conical expansion, A is given by

$$A = \left( \frac{\tan\theta + 1}{\tan\theta} \right) \left( \frac{3\tan\theta}{\pi + 2\pi\tan\theta} \right). \quad (9)$$

The experimentally measured maximum plume length and estimated values of plume length at different pressures are
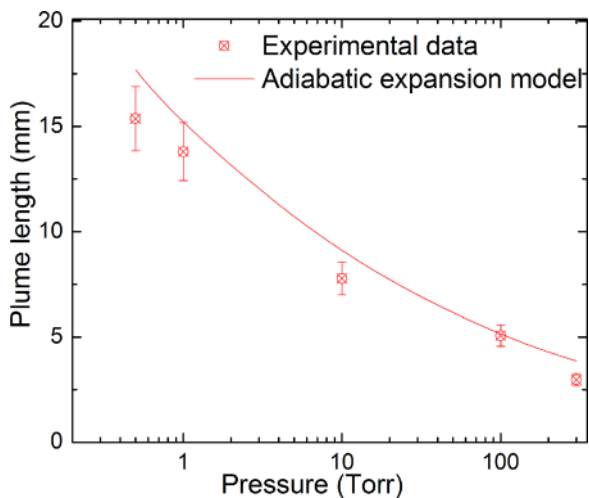


FIG. 9. The estimate plume length vs pressure is given. The symbols represent the experimental measured values of plume length from ICCD images, the solid curve represents the plume length variation with pressure using adiabatic expansion model.

given the Fig. 9. The trend of decreasing plume length with increasing pressure approximately agrees well with adiabatic expansion model especially at moderate to high-pressure values as shown in Figure 9.

## IV. CONCLUSIONS

We investigated the effect of background pressure on expanding nanosecond laser-produced Cu plasma. Optical emission properties, plasma characteristic parameters, hydrodynamics of plume expansion, and surface morphology of laser irradiated area were studied under various pressure levels ranging from vacuum to atmospheric conditions. Background pressure levels significantly control the laser-target and laser-plasma coupling along with hydrodynamics of the resulting plume. Spectral studies showed that continuum background increases with increasing pressure, while the broadening and line intensities increased up to ~100 Torr and then decreased with further increase in pressure. The optimum pressure conditions for analytical applications are noted ~15–30 Torr where the best S/B and S/N was measured. The characteristic plasma parameters were estimated using spectroscopy means and noticed that the excitation temperature peaks at ~300 Torr, while the electron density was maximum ~100 Torr pressure levels. Plasma shielding effect is found to depend on the background pressure, which significantly change the ablation, line and background emission, and S/B.

Surface morphology of irradiated surface showed that the pressure of the ambient gas affects the laser-target coupling significantly because of shielding effect. At higher pressures, the plasma shielding becomes dominant which not only reduce the mass ablation but also absorbs the energy from the incoming laser resulting into higher temperature plasma in front of the target surface. The temperature of plasma produced in front of irradiated surface affects the surface morphology. Evaluation of laser ablated craters suggested that higher melting and splashing at atmospheric pressure levels while the higher material ablation at lower pressure ambient levels. Fast gated images of LPP at a different pressures showed a complex interaction between the plume and ambient leading to changes in the emission and plasma parameters (electron density and temperature) with pressure as well as time. It was observed that the trend of decreasing plume length with pressure approximately was same as predicted by the adiabatic expansion model.

Recently, we reported the role of ambient gas pressure on the expansion and the emission features during ultrafast laser ablation of metal target.[56] Similar to ns LA, the ambient pressure levels were found to affect both the line intensities and broadening along with S/N and S/B ratios and the optimum pressure condition for analytical applications was found to be ∼20–100 Torr. However, comparing with the present results, it can be concluded that the pressure of the ambient gas impacted the ns plume more significantly than the fs LA plume. In fs LA, the ambient gas affected only collisional excitation and confinement, while for ns LA, the background pressure influenced the laser-target and laser-plasma couplings as well as the plume de-excitation mechanisms.

## ACKNOWLEDGMENTS

[1]D. B. Chrisey and G. K. Hubler, *Pulsed Laser Deposition of Thin Films* (John Wiley & Sons Australia, Limited, 1994).

[2]J. J. Gonzalez, A. Fernandez, D. Oropeza, X. Mao, and R. E. Russo, Spectrochim. Acta, Part B **63**, 277 (2008).

[3]D. A. Cremers and L. J. Radziemski, *Handbook of Laser-Induced Breakdown Spectroscopy* (Wiley, 2006).

[4]S. Amoruso, R. Bruzzese, N. Spinelli, R. Velotta, M. Vitiello, X. Wang, G. Ausanio, V. Iannotti, and L. Lanotte, Appl. Phys. Lett. **84**, 4502 (2004).

[5]P. Yeates, J. T. Costello, and E. T. Kennedy, Rev. Sci. Instrum. **81**, 043305 (2010).

[6]S. S. Harilal, T. Sizyuk, A. Hassanein, D. Campos, P. Hough, and V. Sizyuk, J. Appl. Phys. **109**, 063306 (2011).

[7]S. S. Harilal, G. V. Miloshevsky, T. Sizyuk, and A. Hassanein, Phys. Plasmas **20**, 013105 (2013).

[8]N. Farid, H. Wang, C. Li, X. Wu, H. Y. Oderji, H. Ding, and G. Luo, J. Nucl. Mater. **438**, 183 (2013).

[9]A. V. Gusarov, A. G. Gnedovets, and I. Smurov, J. Appl. Phys. **88**, 4352 (2000).

[10]S. S. Harilal, B. O'Shay, Y. Tao, and M. S. Tillack, J. Appl. Phys. **99**, 083303 (2006).

[11]N. L. LaHaye, S. S. Harilal, P. K. Diwakar, A. Hassanein, and P. Kulkarni, J. Appl. Phys. **114**, 023103 (2013).

[12]A. Bogaerts, Z. Y. Chen, and D. Bleiner, J. Anal. At. Spectrom. **21**, 384 (2006).

[13]S. Amoruso, A. Sambri, and X. Wang, J. Appl. Phys. **100**, 013302 (2006).

[14]A. V. Bulgakov and N. M. Bulgakova, J. Phys. D: Appl. Phys. **31**, 693 (1998).

[15]H. Furusawa, T. Sakka, and Y. H. Ogata, J. Appl. Phys. **96**, 975 (2004).

[16]T. E. Itina, J. Hermann, P. Delaporte, and M. Sentis, Phys. Rev. E **66**, 066406 (2002).

[17]S. B. Wen, X. L. Mao, R. Greif, and R. E. Russo, J. Appl. Phys. **101**, 023114 (2007).

[18]Z. Y. Chen and A. Bogaerts, J. Appl. Phys. **97**, 063305 (2005).

[19]W. F. Wei, J. Wu, X. W. Li, S. L. Jia, and A. C. Qiu, J. Appl. Phys. **114**, 113304 (2013).

[20]A. De Giacomo, M. Dell'Aglio, R. Gaudiuso, S. Amoruso, and O. De Pascale, Spectrochim. Acta Part B **78**, 1 (2012).

[21]M. Cirisan, J. M. Jouvard, L. Lavisse, L. Hallo, and R. Oltra, J. Appl. Phys. **109**, 103301 (2011).

[22]S. Mahmood, R. S. Rawat, M. S. B. Darby, M. Zakaullah, S. V. Springham, T. L. Tan, and P. Lee, Phys. Plasmas **17**, 103105 (2010).

[23]S. Mehrabian, M. Aghaei, and S. H. Tavassoli, Phys. Plasmas **17**, 043301 (2010).

[24]S. S. Harilal, J. Appl. Phys. **102**, 123306 (2007).

[25]S. S. Harilal, C. V. Bindhu, M. S. Tillack, F. Najmabadi, and A. C. Gaeris, J. Appl. Phys. **93**, 2380 (2003).

[26]J. A. Aguilera, C. Aragón, and F. Peñalba, Appl. Surf. Sci. **127–129**, 309 (1998).

[27]W. Sdorra and K. Niemax, Microchim. Acta **107**, 319 (1992).

[28]C. B. Dreyer, G. S. Mungas, P. Thanh, and J. G. Radziszewski, Spectrochim. Acta Part B **62**, 1448 (2007).

[29]F. Nazar, B. Shazia, and M. Khaliq, Phys. Scr. **85**, 015702 (2012).

[30]S. S. Harilal, C. V. Bindhu, V. P. N. Nampoori, and C. P. G. Vallabhan, Appl. Phys. Lett. **72**, 167 (1998).

[31]J. R. Freeman, S. S. Harilal, P. K. Diwakar, B. Verhoff, and A. Hassanein, Spectrochim. Acta Part B **87**, 43 (2013).

[32]F. Nazar, S. S. Harilal, H. Ding, and A. Hassanein, Phys. Plasmas **20**, 073114 (2013).

[33]K. F. Al-Shboul, S. S. Harilal, and A. Hassanein, J. Appl. Phys. **113**, 163305 (2013).

[34]B. Verhoff, S. S. Harilal, J. R. Freeman, P. K. Diwakar, and A. Hassanein, J. Appl. Phys. **112**, 093303 (2012).

[35]H. R. Griem, *Spectral Line Broadening by Plasmas* (Academic Press, New York, London, 1974).

[36]I. B. Gornushkin, L. A. King, B. W. Smith, N. Omenetto, and J. D. Winefordner, Spectrochim. Acta Part B **54**, 1207 (1999).

[37]G. Bekefi and W. P. Allis, *Principles Of Laser Plasmas* (John Wiley & Sons Australia, Limited, 1976).

[38]R. Noll, Anal. Bioanal. Chem. **385**, 214 (2006).

[39]S. Yalcn, Y. Y. Tsui, and R. Fedosejevs, J. Anal. At. Spectrom. **19**, 1295 (2004).

[40]J. R. Freeman, S. S. Harilal, B. Verhoff, A. Hassanein, and B. Rice, Plasma Sources Sci. Technol. **21**, 055003 (2012).

[41]R. E. Russo, X. L. Mao, J. H. Yoo, and J. J. Gonzalez, in *Laser-Induced Breakdown Spectroscopy*, edited by J. P. Singh and S. N. Thakur (Elsevier, Amsterdam, 2007), p. 49.

[42]J. J. Chang and B. E. Warner, Appl. Phys. Lett. **69**, 473 (1996).

[43]P. T. Rumsby and J. W. M. Paul, Plasma Phys. **16**, 247 (1974).

[44]L. M. Cabalín and J. J. Laserna, Spectrochim. Acta Part B **53**, 723 (1998).

[45]M. Capitelli, A. Casavola, G. Colonna, and A. De Giacomo, Spectrochim. Acta Part B **59**, 271 (2004).

[46]S. I. Anisimov, D. Bäuerle, and B. S. Luk'yanchuk, Phys. Rev. B **48**, 12076 (1993).

[47]S. Lafane, T. Kerdja, S. Abdelli-Messaci, S. Malek, and M. Maaza, Appl. Phys. A **98**, 375 (2010).

[48]S. S. Harilal, C. V. Bindhu, M. S. Tillack, F. Najmabadi, and A. C. Gaeris, J. Phys. D: Appl. Phys. **35**, 2935 (2002).

[49]T.-J. Andrea and R. Klaus, J. Phys. D: Appl. Phys. **32**, 2827 (1999).

[50]A. K. Sharma and R. K. Thareja, Appl. Phys. Lett. **84**, 4490 (2004).

[51]S. Amoruso, A. Sambri, and X. Wang, Appl. Surf. Sci. **253**, 7696 (2007).

[52]S. George, R. K. Singh, V. P. N. Nampoori, and A. Kumar, Phys. Lett. A **377**, 391 (2013).

[53]N. Arnold, J. Gruber, and J. Heitz, Appl. Phys. A **69**, S87 (1999).

[54]M. R. Predtechensky and A. P. Mayorov, Appl. Superconductivity **1**, 2011 (1993).

[55]P. E. Dyer, A. Issa, and P. H. Key, Appl. Phys. Lett. **57**, 186 (1990).

[56]N. Farid, S. S. Harilal, H. Ding, and A. Hassanein, Appl. Phys. Lett. **103**, 191112 (2013).